ADSORPTION OF SILVER IONS ON CHITOSAN HYDROGEL BEADS

Witold Sujka[1,a], Grzegorz Rogacki[2], Zofia Modrzejewska[2,*], Roman Zarzycki[2]

[1] – Tricomed SA, Świętojańska 5/9 Str., 93–493 Łódź, Poland
[a] – ORCID: 0000–0003–0293–6681
[2] – Faculty of Process and Environmental Engineering, Lodz University of Technology, Wolczanska 213 Str., 93–005 Łódź, Poland
[*]corresponding author: zofia.modrzejewska@p.lodz.pl

Abstract

We investigated the adsorption of silver(I) from silver nitrate ($AgNO_3$) and silver sulphate (Ag_2SO_4). We compared the adsorption ability of chitosan in the form of hydrogel beads with that of chitosan acetate – an initial solution from which the beads were derived. We developed a model of adsorption kinetics, assuming the simultaneous occurrence of the diffusion process and the chemical reaction. We confirmed and described the chemical nature of adsorption based on the Fourier-transform infrared and X-ray photoelectron spectra.

Keywords: *chitosan, gels, adsorption*

Received: 27.04.2023
Accepted: 20.06.2023

1. Introduction

Research on silver is related to the electronic industry and biomedical engineering. Silver recovery is connected with environmental protection and has an economic aspect. The following methods are used to recover silver from liquid-silver-containing substances used for film processing: electrolysis, ion exchange, precipitation, adsorption, and replacement by metals. A variation of ion exchange called ion floatation has also been developed. Silver can also be recovered with various processes. For silver recovery from spent photographic materials (prints, films, etc.) and their wastes, other chemical and biochemical methods are applied instead of incineration pyrolysis. Adsorption on chitosan can also be one of the methods [1–14]. Nevertheless, the particular application of composites with silver is related to biomedical engineering.

Chitosan-silver composites are one of the most effective antimicrobial materials that are not harmful to human cells. Researchers have shown that they have activity against *Staphylococcus aureus*, *Pseudomonas aeruginosa*, *Escherichia coli*, and *Candida albicans*. In biomedical engineering, chitosan-silver systems are mainly used as dressings. They significantly support the healing of wounds and damage caused by oxidative stress [15–20].

The aim of our study was to verify the possibility of using adsorption properties of chitosan in the removal of silver ions. Chitosan, (1–4)–2 amino–2–deoxy–β–D–glucan, is a natural polymer, a product of chitin, (1–4)–2 acetamido–2–deoxy–β–D–glucan, deacetylation. Due to the presence of reactive amino and hydroxide groups, it is used as an adsorbent. In the extensive literature on the adsorption of metal ions onto chitosan, there are only a few publications [6, 7, 12, 13] that refer to silver; hence, this area requires more research attention. We investigated the adsorption of silver from silver nitrate ($AgNO_3$) and silver sulphate (Ag_2SO_4). We compared the adsorption ability of chitosan in the form of hydrogel beads with that of chitosan acetate solution, which was used to produce the beads.

2. Materials and methods

2.1. Characteristics of the Adsorption Beads

Porous chitosan hydrogel beads with a diameter of 3×10^{-3} m were used as an adsorbent. They were produced by the phase inversion method from a 4% chitosan solution with a mean molecular weight 2×10^5 Da and a degree of deacetylation of 68%. The solvent was 4% acetic acid. The beads were formed in up to 10% sodium hydroxide and incubated in it for 24 h. Then, the beads were washed with distilled water until reaching the neutral pH of the water in which they were left.

Figure 1 shows the chitosan hydrogel granules without magnification (upper left image) and their structure seen under an electron microscope. It is characterised by wide pores with diameters ranging from 30 to 300 μm. On the external surface, the pore diameter ranges from 300 to 350 μm. Near the centre, the granule pore diameters decrease to 30–50 μm. However, there are still broad channels compared with the adsorbed ion.

2.2. Description of the Adsorption and Desorption Process for Beads

Silver adsorption was tested in aqueous solutions of $AgNO_3$ and Ag_2SO_4 at a silver concentration of up to 10 mmol/dm^3. Adsorption was carried out in an immobilised bed, in a system combined with a shaker (at an amplitude of oscillation of 8 mm), at 293 K and an initial pH of 5. The adsorbent was 20 g of chitosan beads, which produced about 1 g of pure chitosan. The tests were carried out on 0.25 dm^3 samples – that is, the mass-to-volume ratio was 4:1. The equilibrium concentration for a specific initial concentration was determined after 48 h to produce the adsorption isotherms.

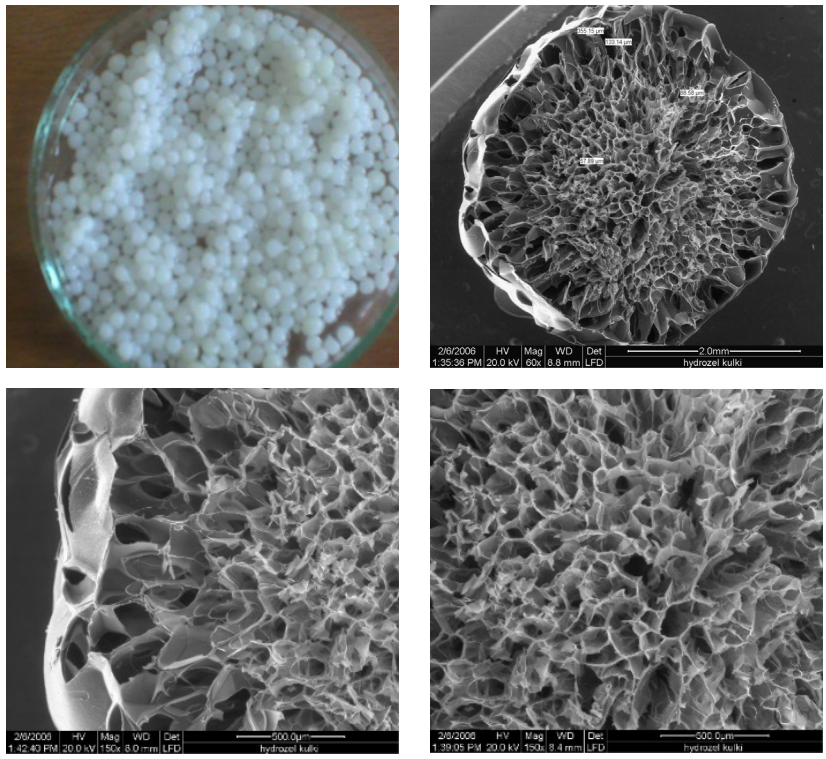

Figure 1. The structure of chitosan beads.

Adsorption was followed by desorption from solutions containing 20 g of humidified chitosan beads and 250 ml of silver solution at an appropriate concentration. Desorption was examined after adsorption of 50 ml of the solution was replaced by 50 ml of distilled water at the same pH as the initial pH of the solutions.

2.3. Description of the Adsorption Process for the Chitosan Acetate Solution

The chitosan hydrogel beads were produced from a 4% chitosan acetate solution. The following procedure was used: to silver solutions with a concentration of 20 and 100 mg silver/dm^3 (0.18 and 9.27 mmol silver/dm^3), 25 ml of chitosan acetate at pH 4 were added. The silver ion concentrations were determined in chitosan acetate solution over time.

2.4. Analytical Methods

The silver ion concentration was determined by using an EAg/S–01 sulphide-silver electrode (Hydromet, Poland) and by inductively coupled plasma emission mass spectrometry.

Structural characteristics of chitosan beads were based on Fourier-transform infrared (FTIR) spectroscopy and X-ray photoelectron spectroscopy (XPS). The FTIR spectra were obtained using a Bio-Rad apparatus (Bio-Rad, Poland) in ATR-FTIR mode, in the range of 4000–500 cm^{-1} with a resolution of 4 cm^{-1} and with 100 scans. The tested samples were pelletised with potassium bromide in a mass ratio of 1:100. The weight of each pellet was approximately 80 mg. XPS spectra were measured using an ESCALAB-210 spectrometer (VG Scientific, USA). A non-chromatised source of X-radiation at 15 kV produced an Al Kα radiation beam (1486.6 eV) with an intensity of 20 mA. The sample was measured after pressing it into a tablet, maintaining a vacuum of 8×10^{-9} mbar in the analytical

chamber of the spectrometer. A survey spectrum was produced at a pass energy in the hemispherical analyser of 75 eV and an energy jump of 0.4 eV. High-resolution spectra in the regions C1s, O1s, and N1s were generated at a pass energy of 20 eV and an energy jump of 0.1 eV. The amount of scavenging in each region was optimised according to the signal intensity.

The collected spectra were analysed with the AVANTAGE software (Thermo Scientific, USA) including nonlinear background, smoothing and fitting the spectra with the use of file shape, which is a sum of the Gauss and Lorentz profile (30:70). The quantitative analysis was performed using the Scofield sensitivity coefficient.

3. Results and Discussion

In this study, we determined the adsorption kinetics and isotherms for chitosan beads, determined the adsorption properties of chitosan acetate and compared it with chitosan beads, and examined structural changes due to adsorption based on the FTIR and XPS spectra.

3.1. Determination of Adsorption Kinetics and Isotherms for Chitosan Hydrogel Beads

Figures 2 and 3 show adsorption over time for $AgNO_3$ and Ag_2SO_4, respectively. We used these data to produce the adsorption isotherms and compared them with the desorption isotherms.

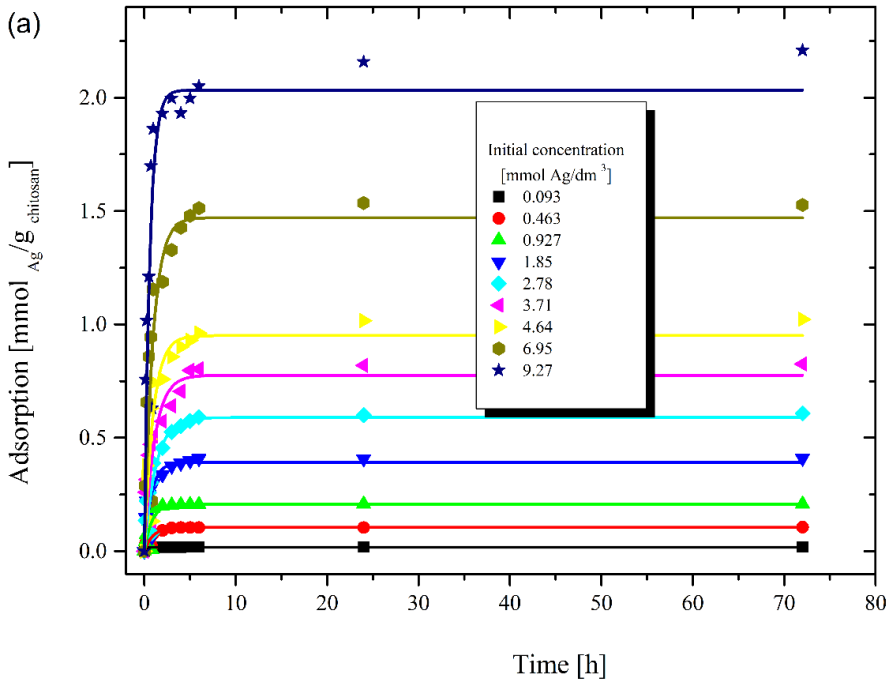

Figure 2. Adsorption of silver ions from silver sulphate over time: (a) change in the silver ion concentration over time, (b) change in the silver ion concentration over time$^{1/2}$ (time 0–1h), and (c) change in the silver ion concentration over time$^{1/2}$ (time 1- 6h).

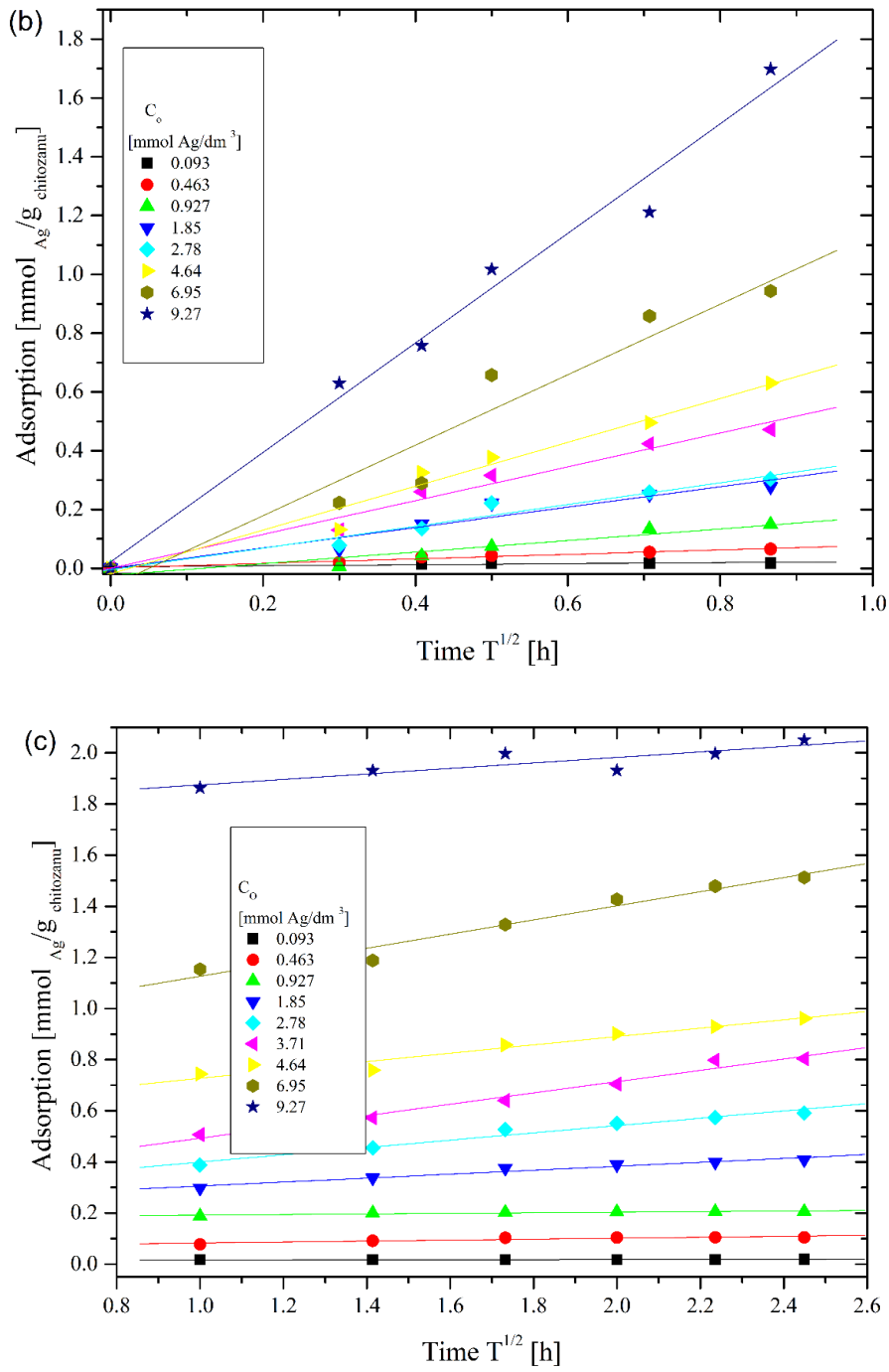

Figure 2. (continued) Adsorption of silver ions from silver sulphate over time: (b) change in the silver ion concentration over time$^{1/2}$ (time 0–1h), and (c) change in the silver ion concentration over time$^{1/2}$ (time 1- 6h).

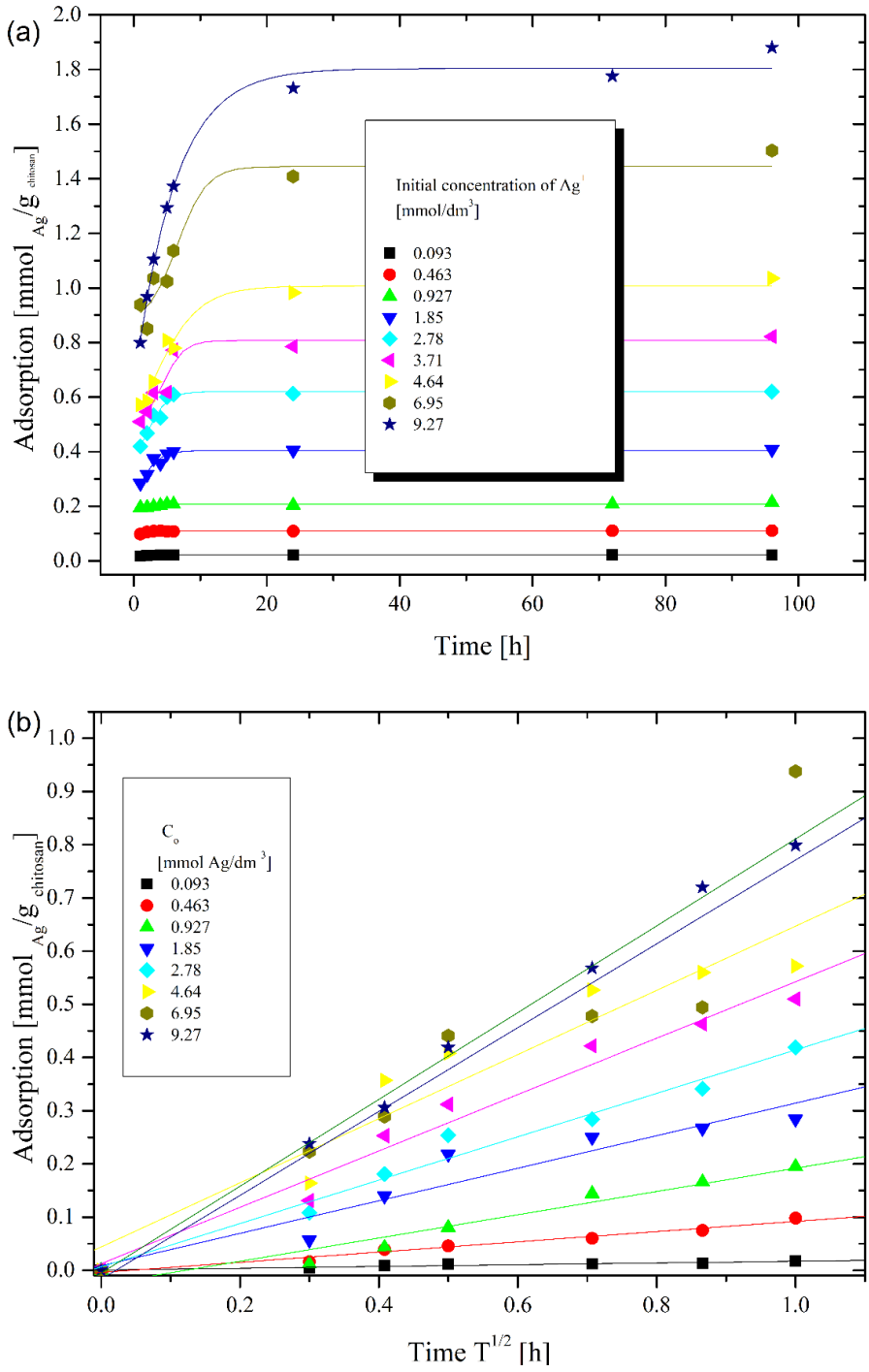

Figure 3. Adsorption of silver ions from silver nitrate over time: (a) change in the silver ion concentration over time, (b) change in the silver ion concentration over time$^{1/2}$ (time 0–1h).

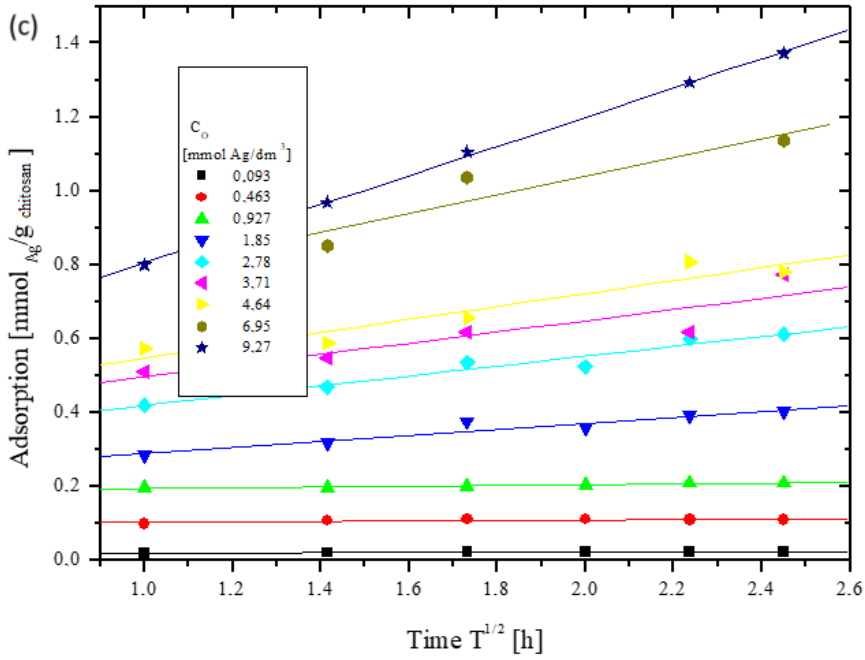

Figure 3. (continued) Adsorption of silver ions from silver nitrate over time: (c) change in the silver ion concentration over time$^{1/2}$ (time 1- 6h).

We determined the rate of adsorption at the tested range of concentrations by using the exponential pseudo first-order equation

$$\frac{da_t}{dt} = k_1(a_e - a_t), \tag{1}$$

or the pseudo second-order equation

$$\frac{da_t}{dt} = k_2(a_e - a_t)^2, \tag{2}$$

which upon integration, assumes the form:

$$a_t = a_m(1 - e^{-kt}) \text{ or} \tag{3}$$

$$a_t = a_e \frac{a_e k_2 t}{1 + a_e k_2 t}. \tag{4}$$

Table 1 shows the parameters of the equations.

Table 1. Parameters of the equations describing the adsorption process over time.

	Pseudo first–order equation			**Pseudo second–order equation**		
	q_e	k_1	**R**	q_e	k_2	**R**
Ag_2SO_4 [mmol/dm³]						
0.093	0.018	10.7	0.92	0.018	1190	0.94
0.463	0.105	1.09	0.84	0.11	14.7	0.85
0.927	0.207	1.2	0.76	0.22	7.79	0.75
1.85	0.392	1.3	0.73	0.42	5.14	0.78
2.78	0.59	0.8	0.88	0.65	1.69	0.88
3.71	0.76	0.9	0.81	0.85	1.54	0.85
4.64	0.95	1.04	0.8	1.04	1.41	0.83
6.95	1.471	1.05	0.82	1.6	0.95	0.84
9.27	2.033	1.68	0.81	2.18	1.19	0.85
$AgNO_3$ [mmol/dm³]						
0.093	0.021	1.7	0.91	0.217	217	0.92
0.463	0.109	2.25	0.91	0.11	78.5	0.87
0.927	0.205	2.9	0.81	0.208	54.9	0.68
1.85	0.393	1.06	0.80	0.41	5.26	0.91
2.78	0.59	0.94	0.77	0.63	2.89	0.91
3.71	0.76	0.74	0.63	0.81	1.5	0.86
4.64	0.95	0.49	0.69	1.01	0.81	0.9
6.95	1.31	1.7	0.49	1.41	0.72	0.75
9.27	1.74	0.36	0.86	1.84	0.3	0.97

Because the models do not reflect fully the process rates and no conclusions can be drawn regarding the mechanisms, we used a model proposed by Weber and Morris. In this model the change of adsorption in time is the function

$$\left(\frac{D \cdot t}{r^2}\right)^{\frac{1}{2}}, \tag{5}$$

where r is the bead radius and D is the effective diffusion coefficient. Linearised curves

$$a_t = f\left(t^{\frac{1}{2}}\right). \tag{6}$$

are illustrated in Figures 2b, 2c, 3b, and 3c. The diffusion coefficient was determined for the first stage of the process (Table 2).

Table 2. Diffusion coefficients at stage I (see Figures 2b and 3b).

Initial concentration	A [mmol/g]		k_i	Diffusion coefficient [m^2/s]	
	$q_{e\infty}$	q_{e1}	mmol/g $s^{0.5}$	A_∞	A_1
0.093	0.018		0.0003	0.96×10^{-10}	
0.463	0.105		0.00127		0.56×10^{-10}
0.927	0.207		0.00328	0.87×10^{-10}	
1.85	0.392	0.28	0.00581	0.74×10^{-10}	1.5×10^{-10}
2.78	0.59	0.42	0.00616		
3.71	0.76	0.5	0.00958		
4.64	0.95	0.55	0.01243	0.6×10^{-10}	1.8×10^{-10}
6.95	1.471		0.01997		
9.27	2.17	0.8	0.031	0.84×10^{-10}	5.3×10^{-10}

The process of adsorption can be divided into three stages:

- rapid adsorption during the first hour (Figures 2b and 3b);
- a slow process lasting from 1–6 h, probably controlled by inner diffusion (Figures 2c and 3c); and
- a very slow stage lasting up to 24 h to reach equilibrium.

In the first hour, silver ions are combined with the reactive groups present in a chitosan molecule ($–NH_2$ and –OH) near the outer bead surface. They can block the pores on the outer surface so that the other silver ions have a longer diffusion path to the active groups that are in the bead structure. Thus, the process slows down as time passes.

To describe the process, we proposed a model combining both mechanisms. We assumed that the process of diffusion inside the granule structure occurs concomitantly with irreversible adsorption on inner granule walls. We made the following assumptions about the model.

- There is simultaneous diffusion of silver ions in the pores of the beads and chemical reactions with the reactive groups of the chitosan molecule.
- The beads have a radius R.
- The distribution of pores and solid material is constant in the granule and does not depend on the radius (we assumed material homogeneity).
- Mass transfer in the granule occurs via diffusion described by Fick's law.
- Adsorption equilibrium occurs on the surface.
- Adsorption is one way (i.e., there is no desorption).
- The diffusion coefficient (D_{AB}) is constant.
- Chemisorption is described by first-order reaction kinetics.

The mass balance of component A (silver ions) of the liquid phase (Ag_2SO_4) consists of the three values:

- stream of diffusion,
- a term related to the chemical reaction,
- term related to accumulation.

The model is described in a previous publication [21].
The mass balance in the liquid phase is:

$$\frac{\partial C_A}{\partial t} = D_{AB}\left(\frac{2}{r}\cdot\frac{\partial C_A}{\partial r} + \frac{\partial^2 C_A}{\partial r^2}\right) - R_A \cdot a_w, \quad (7)$$

$$R_A = k_A (C_A - C_{Aeq}), \tag{8}$$

$$a_w [\frac{m_{ch}^2}{m_p^3}], \tag{9}$$

$$\frac{\partial C_A}{\partial t} = D_{AB}(\frac{2}{r} \cdot \frac{\partial C_A}{\partial r} + \frac{\partial^2 C_A}{\partial r^2}) - k_A \cdot a_w (C_A - C_{Aeq}), \tag{10}$$

$$k_V = k_A \cdot a_w. \tag{11}$$

The mass balance in the solid phase is:

$$dm \cdot \frac{dq}{dt} = R_A \cdot a_w \cdot \varepsilon \cdot dV, \tag{12}$$

$$dV = 4 \cdot \pi \cdot r^2 \cdot dr, \tag{13}$$

$$dm = dV (1-\varepsilon) \cdot \rho_{ch}, \tag{14}$$

$$\frac{dq}{dt} = \frac{a_w \cdot \varepsilon}{(1-\varepsilon) \cdot \rho_{ch}} \cdot k_A (C_A - C_{Aeq}). \tag{15}$$

The initial boundary conditions for the liquid phase in the beads are:

$$t = 0 \qquad C_A = 0, \tag{16}$$

$$r = 0 \qquad \frac{dC_A}{\partial r} = 0, \tag{17}$$

$$r = R \qquad C_A = C_{Af}. \tag{18}$$

The initial boundary conditions for the solid phase in the beads are:

$$t = 0 \qquad q = 0. \tag{19}$$

The boundary condition for the surface of the beads is:

$$V_f \cdot \frac{\partial C_f}{\partial t} = -4 \cdot \pi \cdot R^2 \cdot \alpha \cdot n \cdot D_{AB} \cdot \left.\frac{\partial C}{\partial r}\right|_{r=R}. \tag{20}$$

At the boundary of phase separation in the beads

$$C_{Aeq} = f(q_e). \tag{21}$$

Figure 4 show the verification of the model, that is, changes in the silver ion concentration over time for various initial concentrations of the adsorbent. The experimental data are marked with points, and the lines are the result of solving the model equations. The constant describing the adsorption process according to the proposed model – that is, the constant of the surface interaction at the determined diffusion coefficient $D_{AB} = 1.13 \cdot 10^{-9} \frac{m^2}{s}$ is presented in Table 3.

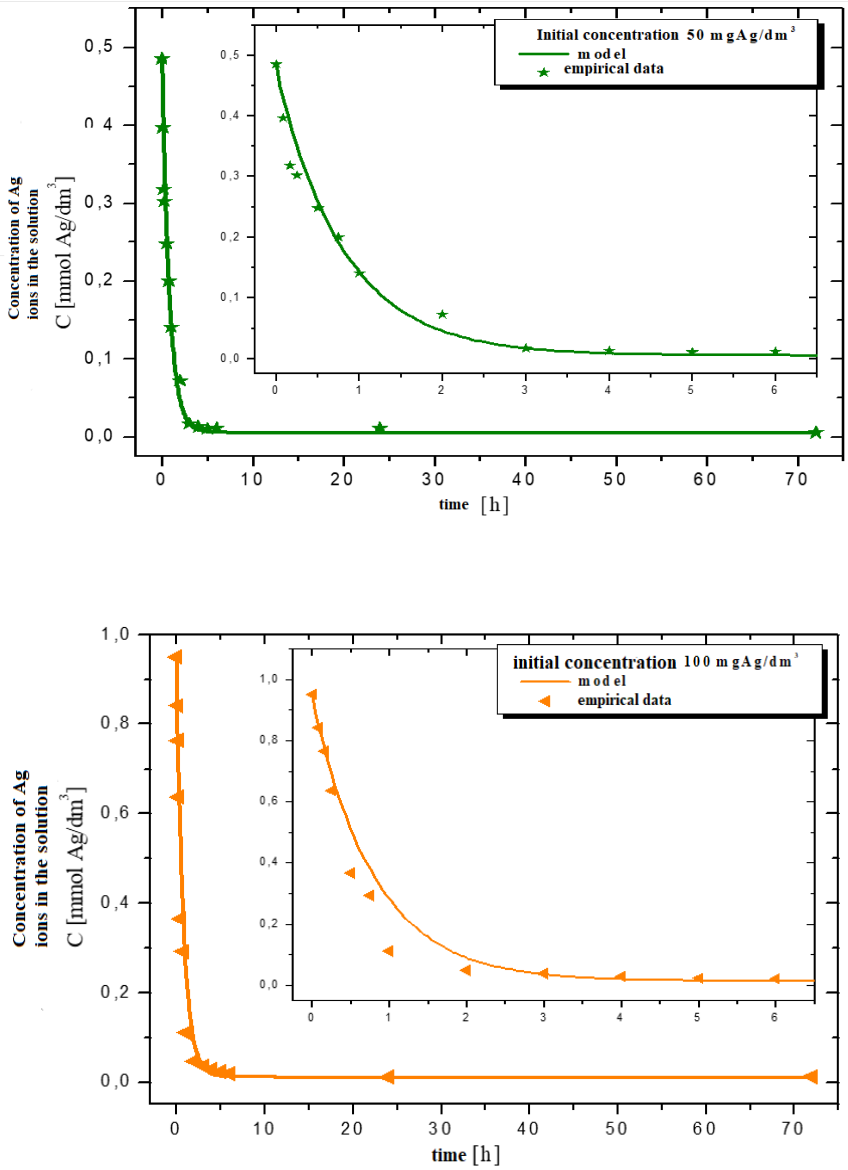

Figure 4. Verification of the model. Change in the silver ion concentration over time with different initial C_{Ag}: (dark green) 50 mg_{Ag}/dm^3, (orange) 100 mg_{Ag}/dm^3.

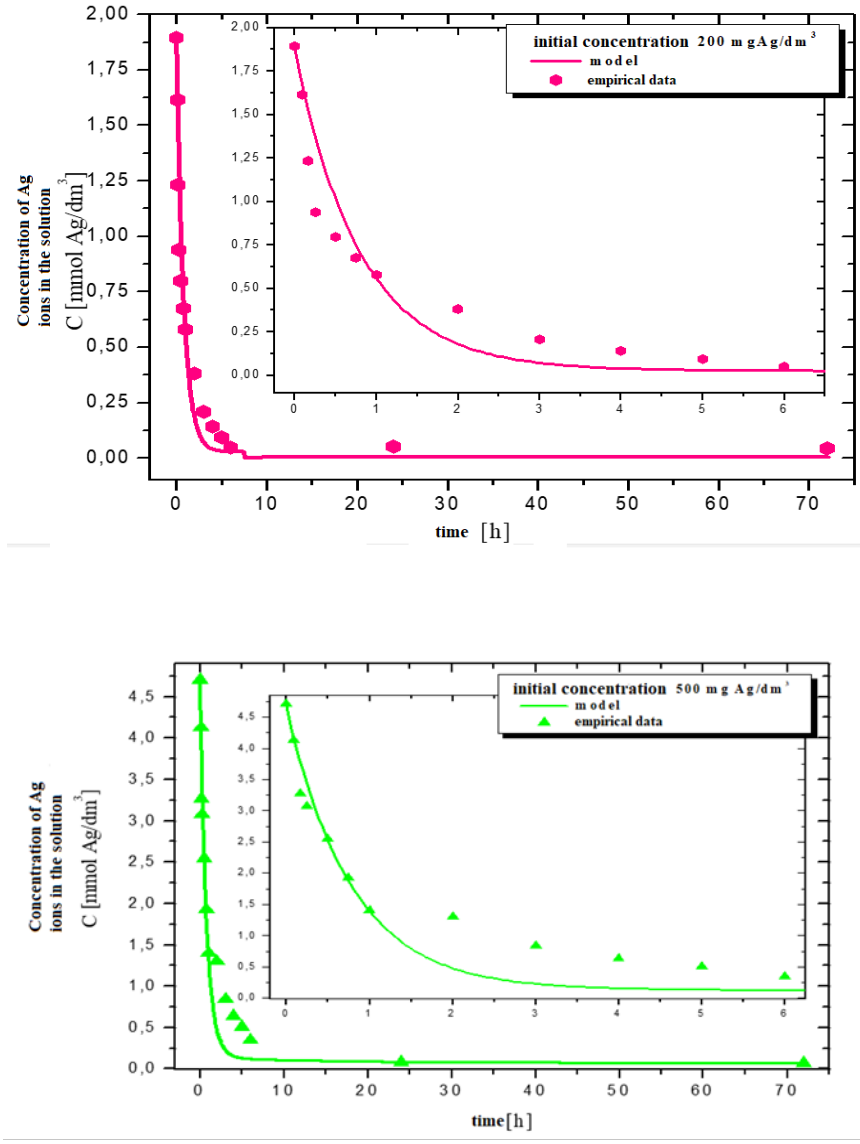

Figure 4. (continued) Verification of the model. Change in the silver ion concentration over time with different initial C_{Ag}: (pink) 200 mg_{Ag}/dm^3, (light green) 500 mg_{Ag}/dm^3.

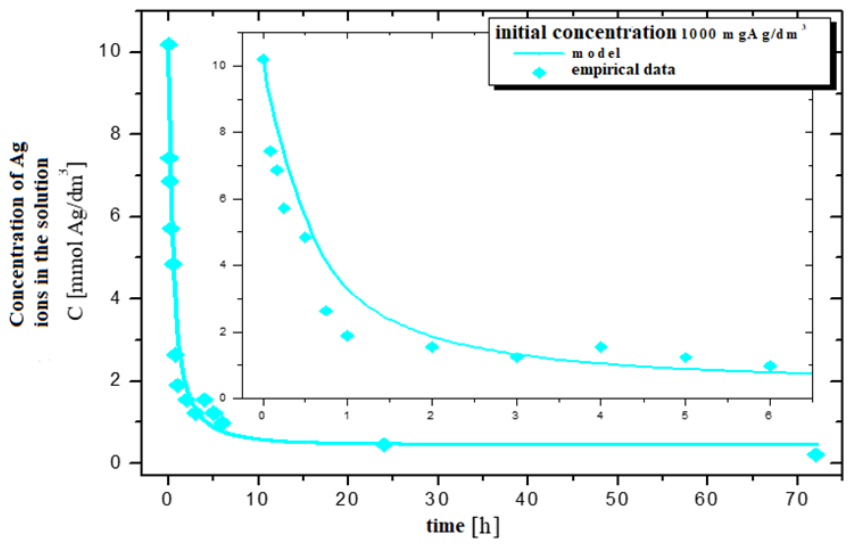

Figure 4. (continued) Verification of the model. Change in the silver ion concentration over time with different initial C_{Ag}: (blue) 1000 mg_{Ag}/dm^3.

Table 3. Mass transfer coefficient k for individual processes.

Initial concentration [mg silver/dm³]	Constant k [1/s]	Sum of the errors
50	2×10^{-3}	0.0361
100	2.4×10^{-3}	0.0149
200	1.6×10^{-3}	0.123
300	1.4×10^{-3}	0.0391
400	1.4×10^{-3}	0.121
500	1.8×10^{-3}	0.0822
750	2×10^{-3}	0.0458
1000	2.6×10^{-3}	0.0469
	1.9 × 10–3	

The model provides a good description of the adsorption of silver ions, with an average constant k of 1.9×10^{-3} [1/s]. The values for k obtained for low concentrations have a higher error, probably due to the dominating surface nature of the process in these cases. Overall, the proposed model describes the processes of ion adsorption on chitosan and can be used successfully to simulate these processes.

We determined the isotherms by assuming that equilibrium occurs by 48 h based on the Langmuir and Freundlich equations (Figures 5 and 6). The Langmuir equations (L) is:

$$q_e = \frac{k \cdot C_e \cdot a}{1 + k \cdot C_e}, \tag{22}$$

and the Freundlich equations (F) is:

$$q_e = k \cdot C_e^{\,n}. \tag{23}$$

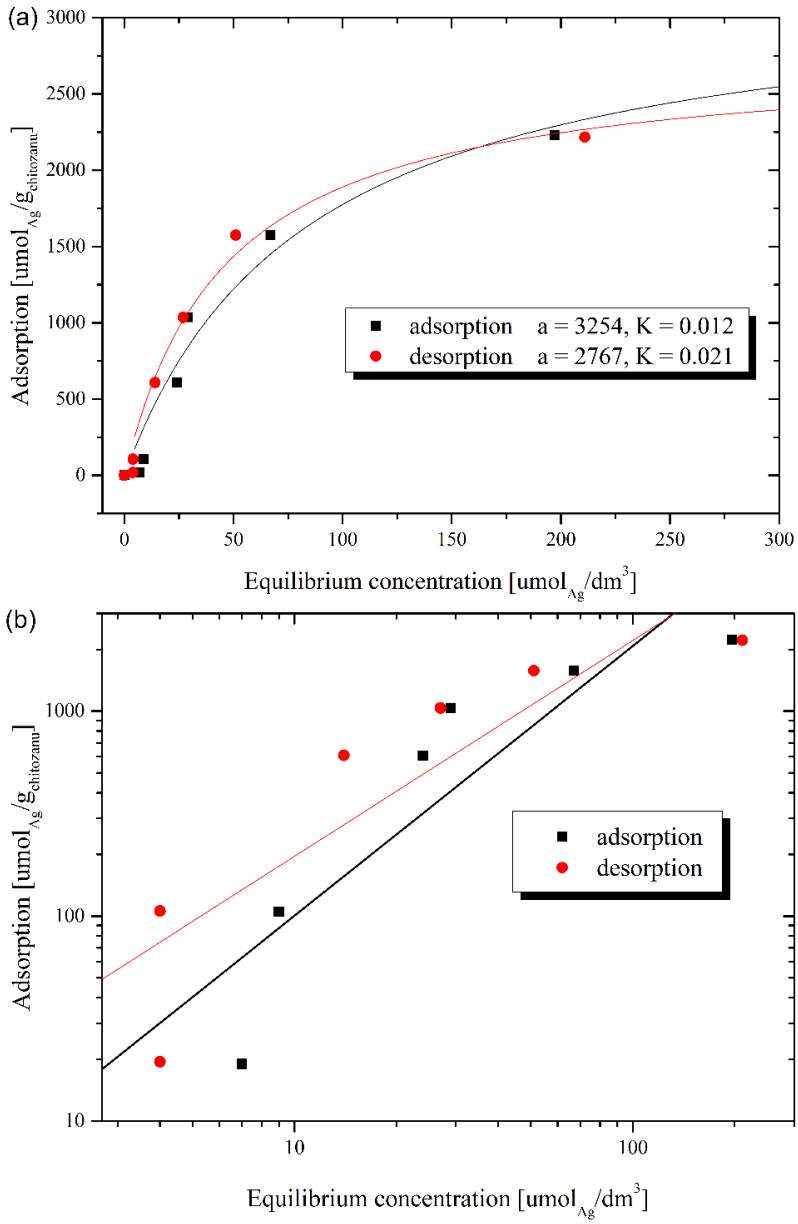

Figure 5. Adsorption-desorption isotherm of silver from silver sulphate calculated with (a) the Langmuir equation and (b) the Freundlich equation.

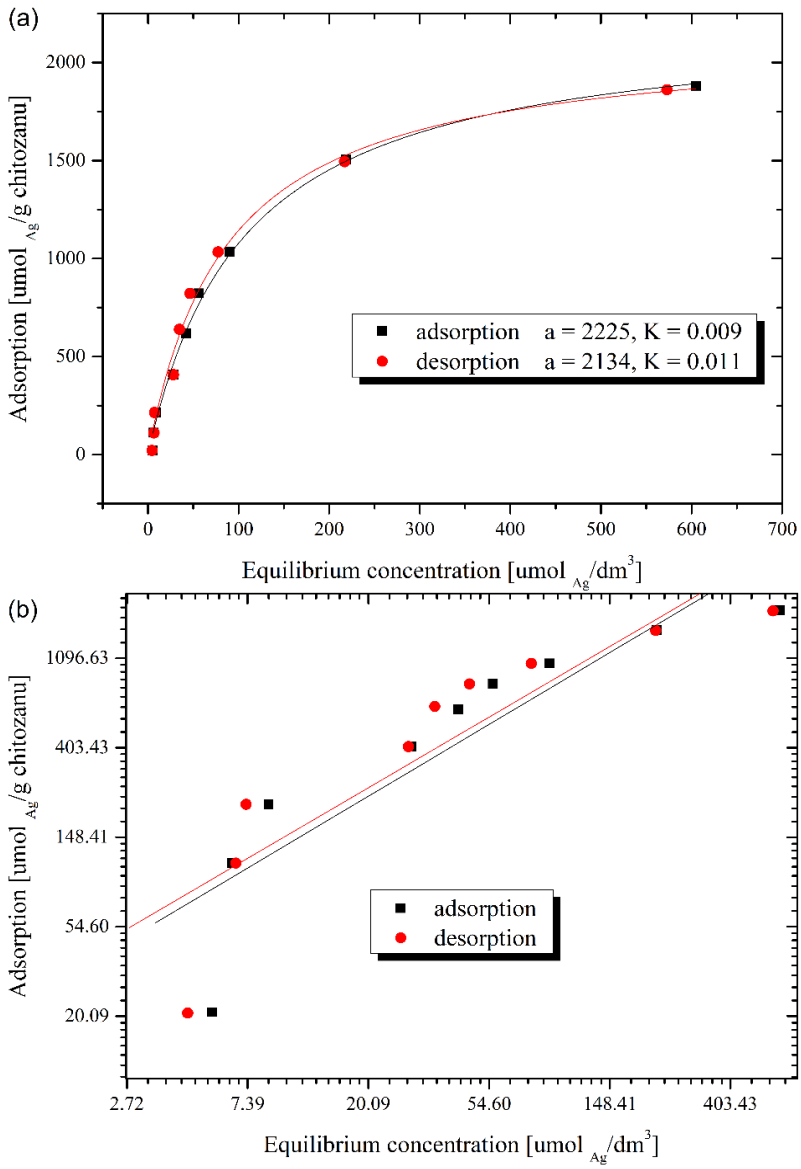

Figure 6. Adsorption-desorption isotherm of silver from silver nitrate calculated with (a) the Langmuir equation and (b) the Freundlich equation.

We found that chitosan beads have good absorption properties regarding silver ions. The adsorption isotherms in the range of low equilibrium concentrations (up to 10 mmol silver/dm^3) are well described by the Langmuir isotherms. There is slightly higher adsorption of silver ions Ag_2SO_4. The adsorption isotherms overlap with the desorption isotherms, which is an evidence that the process has a chemical character.

The equilibrium adsorption of silver ions is about 3 mmol/g chitosan for Ag_2SO_4 and 2.2 mmol/g chitosan for $AgNO_3$. The constant K, which reflects the interrelationship between the adsorbent and adsorption, is practically the same for Ag_2SO_4 and $AgNO_3$ and is equal to 0.01. There is a higher constant for desorption (for Ag_2SO_4). This finding confirms that the process has a chemical character.

For comparison, we also evaluated the adsorption of silver ions in the chitosan acetate solution, considering the same amount of chitosan acetate we used to prepared the beads (Figures 7 and 8). We found that the chitosan beads had better adsorption properties. The lower adsorption for chitosan salts is probably due to the presence of protonated amino groups in chitosan. When the silver ion concentrations in the solution are low, the complex between chitosan salt and silver ions is not stable.

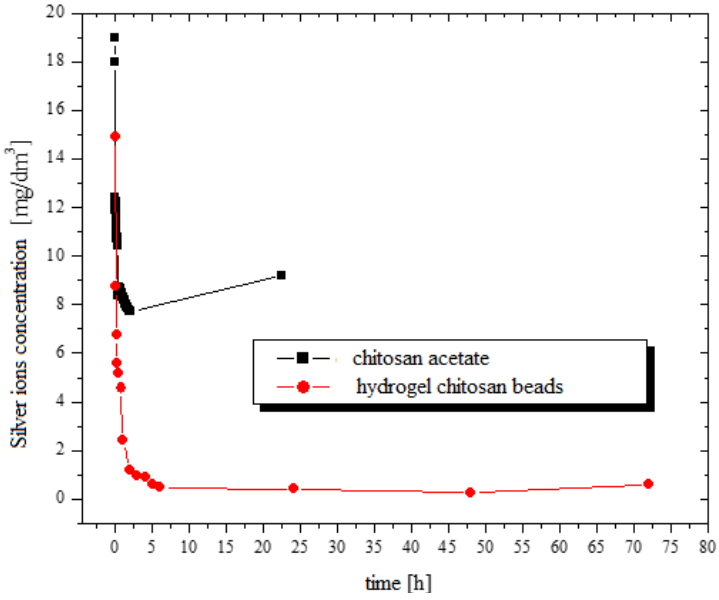

Figure 7. Change in the silver ion concentration (from 20 mg/dm^3 silver nitrate) over time from chitosan acetate and chitosan beads.

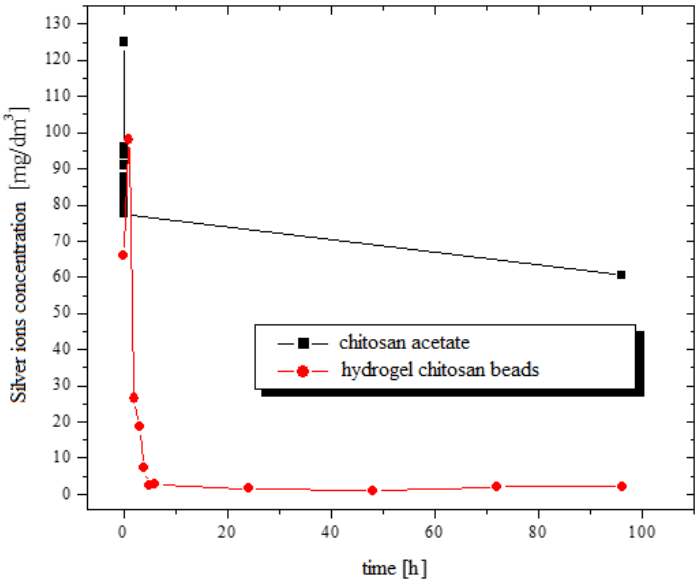

Figure 8. Change in the silver ion concentration (from 100 mg/dm^3 silver nitrate) over time from chitosan acetate and chitosan beads.

3.2. Structural Evaluation

3.2.1. Analysis of FTIR Spectra

We used FTIR spectroscopy to examine the chemical character of adsorption. The spectra are presented in Figures 9 and 10.

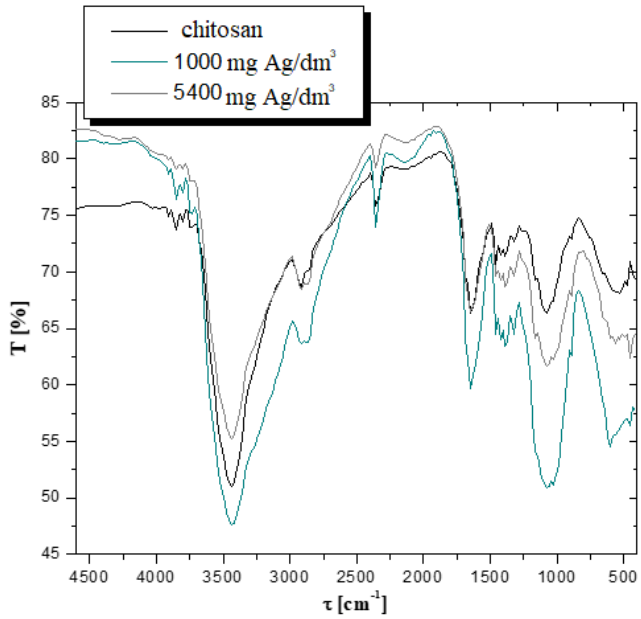

Figure 9. Fourier-transform infrared spectrum of chitosan-silver ions at 4500–500 cm^{-1}.

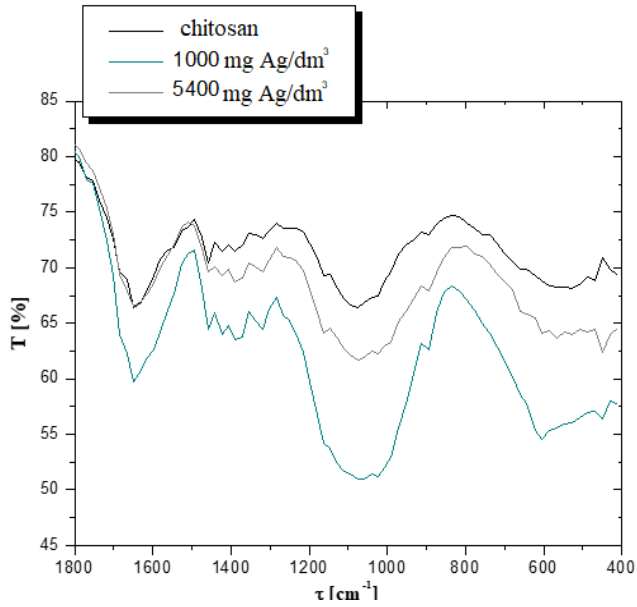

Figure 10. Fourier-transform infrared spectrum of chitosan-silver ions at 1800–400 cm^{-1}.

We noted a change in the shape of a broad band whose maximum is at 3500 cm^{-1}. This may provide evidence of the interaction between the $–NH_2$ and –OH groups of chitosan with silver ions, namely an increase in intramolecular interactions and hydrogen bonds. The two peaks at 2870 and 2900 cm^{-1}, probably coming from C–N, are equalised. The peaks are related to symmetric or asymmetric CH_2 stretching attributed to the pyranose ring. There are bands characteristic of N–acetylated amine at 1660 cm^{-1} (C=O) and 1560 cm^{-1} (N–H bending vibration in the $–NH_2$ group), which correspond to the primary and secondary amines. The broad band with a maximum at 1590 cm^{-1} is a typical amine peak. This spectrum can be overlapped by bands that come from the primary amines at 1660 cm^{-1} and carboxyl groups at 1568 cm^{-1} as well as protonated amino groups (NH_3^+) at 1630 cm^{-1}. Changes in the amide I and II bands indicate the participation of amino groups in the formation of the chitosan-silver ion complexes. The participation of $–CH_2OH$ groups is very likely, as indicated by changes at 1420 cm^{-1}. There are also changes at 1370 cm^{-1} related to $C–CH_3$ deformations in the amide groups. It seems that the saccharide structure undergoes some changes: after adsorption of silver ions, the peak at 1050 cm^{-1} becomes more visible. There is also a change for the bands characteristic of $–CH_3COH$ groups (850 and 840 cm^{-1}) and a saccharide structure, that is, 890 and 1150–1040 cm^{-1}. The band related to the presence of oxygen bridges (O–C–O) at 1050 cm^{-1} is equalised with the band at 1150 cm^{-1}, and the bands at 850 and 840 cm^{-1} are combined. This may be evidence of stable b-glucosamine bonds between glucosamine and *N*–acetylamine molecules and of bonds with $–CH_3COH$ groups. Finally, there are changes in the low-frequency range (650–400 cm^{-1}). These changes may result from the reducing effect of chitosan and the precipitation of metallic silver.

3.2.2. Analysis of XPS Spectra

We analysed the XPS spectra for oxygen, carbon and nitrogen, as shown in Tables 4, 5, and 6, respectively.

Table 4. Analysis of X-ray photoelectron spectra for oxygen after adsorption of silver ions.

Oxygen	Chitosan beads		Chitosan beads + silver 4.16/1.37		Chitosan beads + silver 7/3.12	
	Energy binding [eV]	Group participation [%]	Energy binding [eV]	Group participation [%]	Energy binding [eV]	Group participation [%]
H_2O, β(1→4)	534.53	1.6	534.69	0.74	534.85	0.91
C–OH, CH_2OH	533.16	15.6	533.21	11.7	532.32	9.71
C–O–C	532.46	10.59	532.49	9.9	531.92	9.22
NH–(C=O)–C	531.26	2.98	531.06	5.43	529.41	4.63
Sulphate oxygen (SO_4)			532.5	5.56	532.57	10.27
Total		30.77		38.36		40.71

Interpretation of the spectra after adsorption of oxygen ions is difficult due to the presence of additional oxygen from the SO_4 group. This can explain the increase in the total oxygen content in the sample. We considered this oxygen in the amount to be stoichiometric to the amount obtained from the analysis of adsorbed copper ions. As the amount of silver adsorbed on chitosan increases, the per cent contribution of C–OH groups decreases.

During adsorption, the peak identified for the C=O groups shifts towards lower energies and the percent contribution of these groups increases. This phenomenon can be explained by the oxidation of metal on the surface. It seems that this oxidation occurs to a greater extent when the initial concentration of the adsorbent in 1 g/dm^3 rather than 10 g/dm^3.

After adsorption of silver ions, there is a slight decrease in the percent share of C–O–C groups, which may suggest the destruction of (1→4)β–glycosidic bonds or the share of oxygen present in the saccharide ring. This latter view is unlikely but has been suggested by Braier and Jishithe [22].

To sum up:

- OH groups are involved in the formation of chitosan-silver ion complexes;
- (1→4)β-glycosidic bonds are likely broken; and
- silver oxidation occurs on the surface.

Table 5. Analysis of X-ray photoelectron spectra for carbon after adsorption of silver ions.

Carbon	Chitosan beads		Chitosan beads + silver 4.16/1.37		Chitosan beads + silver 7/3.12	
	Energy binding [eV]	Group participation [%]	Energy binding [eV]	Group participation [%]	Energy binding [eV]	Group participation [%]
N–C=O	288.84	2.34	288.86	2.2	288.57	4.13
C=O, O–C–O	287.84	9.81	287.88	8.08	287.56	6.73
C–OH, C–O–C	286.43	30.68	286.43	26.66	286.42	23.73
C–NH_2	285.43	10.48	285.72	6.61	284.79	4.52
C–C–, –C–H	284.6	10.06	284.6	11.27	284.6	7.36
Total		62.25		54.82		46.47

The analysis of the carbon spectra indicates significant participation of amino groups in the formation of silver-chitosan complexes. There is a significant decrease in the percent of C–NH_2 groups that is proportional to the increase in the amount of adsorbed silver. We noted a similar tendency for the C–OH groups. There are changes at carbon C1 (O–C–O) – their percentage decreases – that may suggest very unlikely attachment of silver ions to C1 after chain breakage or unlikely oxygen present in the saccharide ring [22].

To sum up:

- the XPS spectra for carbon confirm the conclusion from the oxygen spectra that C-NH_2 groups are involved in the formation of chitosan-silver complexes, and that OH groups are also reactive, but in the case of silver the share of OH groups seems to be more significant.

Table 6. Analysis of X-ray photoelectron spectra for nitrogen after adsorption of silver ions.

Nitrogen	Chitosan beads		Chitosan beads + silver 1.85/3.84		Chitosan beads + silver 2.63/4.88	
	Group participation [%]	Energy binding [eV]	Group participation [%]	Group participation [%]	Energy binding [eV]	Group participation [%]
C–NH_3^+	401.97	0.26	401.79	1.32	401.80	1.9
O=C–N	400.48	1.35	400.16	1.16	400.32	1.08
C–NH_2	399.17	5.39	399.49	2.3	399.17	2
Total		7		4.78		4.98

The nitrogen spectra clearly indicate the participation of C–NH_2 amino groups in the adsorption process of silver ions and the protonation of amino groups. The amount of NH_3^+ increases as the amount of adsorbed silver ions increases. On the other hand, there is no change in the percentage of O=C–N content, which may suggest the non-reactivity

of acetylamino groups in the formation of chelate compounds with silver. In the case of silver ion adsorption, the OH group is the most reactive, while the NH_2 group is slightly less reactive towards silver ions. There are changes in the O–C–O groups.

4. Conclusions

We drew the following conclusions from our research:

1. Chitosan hydrogel beads show greater adsorption than chitosan in the form of a salt, namely chitosan acetate.
2. The adsorption ability of chitosan hydrogel beads towards silver ions depends slightly on the presence of co-ions.
3. The process of adsorption in the first hour is probably dominated mainly by a chemical reaction, and then controlled by the diffusion inside a porous hydrogel structure.
4. The process of silver ion adsorption is well described by the proposed model assuming simultaneous occurrence of both diffusion and a chemical reaction in the adsorption process.
5. The XPS and FTIR spectra confirm that the C-NH_2 and OH groups are involved in the formation of chitosan-silver ion complexes. They most likely form due to the breaking of (1→4)β-glycosidic bonds, alongside silver oxidation on the surface.
6. Chitosan granules are an interesting silver adsorbent. Due to the reducing effect of chitosan, it is possible to obtain an adsorbent for metallic silver, which may be of significant importance in both environmental and biomedical engineering.

5. Designations of the Terms and Constants in the Equations

The pseudo-first order and pseudo-second order equations:

q – temporary adsorption [mmol ions/g chitosan],
q_e – equilibrium adsorption [mmol ions/g chitosan],
t – time [h],
k_1 – adsorption rate constant [1/h],
k_2 – adsorption rate constant [g chitosan/mmol ions·h].

The model we proposed in this study:

a_w – development of the inner surface of chitosan per unit volume of fluid

$$\frac{m_{ch}^2}{m_p^3},$$

R_A – reaction rate of the surface process related to the surface unit of the solid body

$$\frac{molA}{m_{ch}^2 \cdot s},$$

k_A – surface process rate constant $\frac{m_p^3}{m_{ch}^2 \cdot s}$,

ρ_{ch} – chitosan density, $\frac{kg_{ch}}{m_{ch}^3}$,

α – the fraction of the surface of the sphere open to diffusion,
n – the number of beads,
V_f – bath volume, m^3,
C_f – concentration of component A in the bath,

C_{f0} – initial bath concentration $\frac{\text{molA}}{\text{m}_\text{p}^3}$.

The Langmuir and Freundlich equations:
k – Langmuir equilibrium constant [dm^3/mmol],
a – sorption capacity [mmol/g],
q_e – equilibrium concentration in the solid phase (surface) [mmol/g],
C_e – equilibrium volumetric concentration in solution [mmol/dm^3],
K – Freundlich constant,
n – Freundlich exponent.

6. References

[1] Muzzarelli RAA; (1973) Natural Chelating Polymers. Pergamon, Oxford.
[2] Bailey SE, Olin TJ, Bricka RM, Adrian DD; (1999) A review of potentially low-cost sorbents for heavy metals. Wat Res 33, 2469–2479. **DOI:**10.1016/S0043–1354(98)00475–8
[3] Yoshizuka K, Lou Z, Inoue K; (2000) Silver-complexed chitosan microparticles for pesticide removal. React Funct Polym 44, 47–54. **DOI:**10.1016/S1381–5148(99)00076–0
[4] Wu FC, Tseng RL, Juang RS; (2000) Comparative adsorption of metal and dye on flake and bead-types of chitosans prepared from fishery wastes. J Hazard Mater B73, 63–75. **DOI:**10.1016/s0304–3894(99)00168–5
[5] Ying Y, Wang Y, Liu H; (2003) Preparation of new crosslinked chitosan with crown ether and their adsorption silver ion for antibacterial activities. Carbohydr Polym 53, 425–430. **DOI:**10.1016/S0144–8617(03)00104–8
[6] Varma AJ, Deshpande SV, Kennedy JF (2004) Metal complexation by chitosan and its derivatives: a review. Carbohydr Polym 55, 77–93. **DOI:**10.1016/j.carbpol.2003.08.005
[7] Jia YF, Steele CJ, Hayward IP, Thomas KM; (1998) Mechanism of adsorption of gold and silver species on activated carbons. Carbon 36, 1299–1308. **DOI:**10.1016/S0008–6223(98)00091–8
[8] Hidefumi S, Ishikawa J, Koike M, Doi K, Wada H; (2003) Adsorption and concentration of silver ion with polymer-supported polythiazaalkane resins. React Funct Polym 55, 299–310. **DOI:**10.1016/S1381–5148(03)00021-X
[9] Russo T, Fucile P, Giacometti R, Sannino F; (2021) Sustainable removal of contaminants by biopolymers: a novel approach for wastewater treatment. Current state and future perspectives. Processes 9, 719. **DOI:**10.3390/pr9040719
[10] Sumaila AO, Sumaila AS, Abdullahi AS, Usman AO, Ekwoba L; (2022) Application of chitosan-silver nanocomposites for heavy metals removal: a review study. J Mater Environ 13, 869–883.
[11] Bhatt P, Joshi S, Urper Bayram GM, Khati P, Simsek H; (2023) Developments and application of chitosan-based adsorbents for wastewater treatment. Environ Res 226, 1115530. **DOI:**10.1016/j.envres.2023.115530

[12] Engidayehu A, Sahu O; (2020) Enzymatic recovery of silver from waste radiographic film: optimize with response surface methodology. Sustain Chem Pharm 15, 100224. **DOI:**10.1016/j.scp.2020.100224

[13] Modrzejewska Z, Dorabialska M, Zarzycki R, Wojtasz-Pająk A; (2009) The mechanism of sorption of Ag+ ions on chitosan microgranules: IR and NMR studies. Prog Chem Appl Chitin Deriv XIV, 49–64.

[14] Modrzejewska Z, Biniaś D, Wojtasz-Pająk A, Dorabialska M, Zarzycki R; (2008) Crystalline structure of chitosan microgranules cross-linked with Cu^{2+} and Ag^{+} ions. Cryst Growth Des 8, 4372–4377. **DOI:**10.1021/cg700906y

[15] Chen J, Fan L, Yang C, Wang S, Zhang M, Xu J, Luo S; (2020) Facile synthesis of Ag nanoparticles-loaded chitosan antibacterial nanocomposite and its application in polypropylene. Int J Biol Macromol 161, 1286–1295. **DOI:**10.1016/j.ijbiomac.2020.07.151

[16] Hajji S, Khedir SB, Hamza-Mnif I, Hamdi M, Jedidi I, Kallel R, Boufi S, Nasri M; (2019) Biomedical potential of chitosan-silver nanoparticles with special reference to antioxidant, antibacterial, hemolytic and in vivo cutaneous wound healing effects. Biochim Biophys Acta Gen Subj 1863, 241–254. **DOI:**10.1016/j.bbagen.2018.10.010

[17] Regiel-Futyra A, Kus-Liśkiewicz M, Sebastian V, Irusta S, Arruebo M, Kyzioł A, Stochel G; (2017) Development of noncytotoxic silver–chitosan nanocomposites for efficient control of biofilm forming microbes, RSC Adv 7, 52398–52413. **DOI:**10.1039/c7ra08359a

[18] Latańska I, Rosiak P, Paul P, Sujka W, Kolesińska B; (2023) Modulating the physicochemical properties of chitin and chitosan as a method of obtaining new biological properties of biodegradable materials. In: Chitin and Chitosan – Physicochemical Properties and Industrial Applications. IntechOpen, London. **DOI:**10.5772/intechopen.95815

[19] Latańska I, Kolesińska B, Draczyński Z, Sujka W; (2020) The use of chitin and chitosan in manufacturing dressing materials. Prog Chem Appl Chitin Deriv XXV, 260–272. **DOI:**10.15259/PCACD.25.00

[20] Paul P, Kolesińska B, Sujka W; (2019) Chitosan and its derivatives – biomaterials with diverse biological activity for manifold applications. Mini Rev Med Chem 19, 737–750. **DOI:**10.2174/1389557519666190112142735

[21] Modrzejewska Z, Rogacki G, Sujka W, Zarzycki R; (2016) Sorption of copper by chitosan hydrogel: Kinetics and equilibrium. Chem Eng Process Intensif 109, 104–113. **DOI:**10.1016/j.cep.2016.08.014

[22] Braier NC, Jishi RA; (2000) Density functional studies of Cu^{2+} and Ni^{2+} binding to chitosan. J Mol Struct 1–3, 51–55. **DOI:**10.1016/S0166–1280(99)00288–2